

Bias Driven Non-Equilibrium Phase Transitions

José Afonso

Instituto de Plasmas e Fusão Nuclear, Instituto Superior Técnico, Av. Rovisco Pais 1, Lisbon, Portugal

Pedro Ribeiro

*CeFEMA, Instituto Superior Técnico, Universidade de Lisboa Av. Rovisco Pais, 1049-001 Lisboa, Portugal and
Beijing Computational Science Research Center, Beijing 100193, China*

Stefan Kirchner

Department of Electrophysics, National Yang Ming Chiao Tung University, Hsinchu 30010, Taiwan

We investigated bias-driven non-equilibrium quantum phase transitions in a paradigmatic transport setup consisting of a quantum dot, with an interacting charging energy, connected to non-interacting leads. We mapped out the non-equilibrium zero-temperature phase diagram as a function of interaction strength and bias voltage across the dot. Our central results are the behavior of charge susceptibility and current noise near the phase transition. Specifically, we show that zero-frequency current fluctuations become critical and diverge as $|V - V_c|^{-2}$ near the non-equilibrium critical points. The charge susceptibility also diverges at the transition. These results are achieved using a Random Phase Approximation (RPA). We validated our findings in the high voltage limit, where the system-leads interaction becomes *Markovian*, using the *Lindblad* equation. At this limit, both the average current and current noise coincide with those of a non-interacting system, consistent with the RPA effective field theory. Our research demonstrates that current noise is a valuable tool for detecting and probing critical fluctuations at quantum critical points. It also opens new pathways for studying other types of non-equilibrium voltage-driven transitions.

Keywords: electron transport, quantum dot, quantum phase transitions, non-equilibrium dynamics

I. INTRODUCTION

The study of quantum phase transitions has mainly focused on equilibrium scenarios. However, the intricate landscape of non-equilibrium quantum phase transitions poses fundamental questions that are largely unexplored.

Our investigation revolves around a quantum dot, a nanoscale system that exhibits quantum phenomena. Quantum dots provide a powerful means of studying and manipulating systems undergoing quantum phase transitions, as they can confine electrons in all three spatial dimensions and could have quantized energy levels akin to those in atoms [1]. This makes them excellent systems for studying quantum phase transitions, as changes in their energy levels under various conditions can be more easily observed and measured.

In electronic experiments, whose theoretical modulation constitutes a central topic of investigation, the quantum dots are coupled to metallic leads. These leads act as reservoirs of electrons and are connected to an external circuit, allowing for current flow through the quantum dot [1]. Moreover, a voltage bias is applied across the leads, creating a difference in chemical potential between them. As a result, the *Fermi* levels do not align, which drives the flow of electrons from the higher *Fermi* level to the lower one [2].

This continuous flow of charge is inherently a non-equilibrium process, representing a steady state of ongoing energy and particle exchange rather than a state of thermodynamic equilibrium [1]. If we have a closed sys-

tem in equilibrium, energy exchange within the system eventually ceases, and the system would reach a thermal equilibrium state. However, in this case, we have an ongoing exchange of energy and particles that makes the system open and prevents the system from reaching equilibrium [3].

Furthermore, these experiments are conducted at very low temperatures since the quantum effects dominate only at these temperatures as we reduce the thermal noise.

General Theoretical Framework

Due to their inherent open and out-of-equilibrium nature, studying our non-equilibrium system demands a framework distinct from traditional equilibrium scenarios. The *Keldysh* functional integral is a powerful and comprehensive tool for addressing non-equilibrium problems, which is widely explained in [4–10].

As a result, this formalism provides us with the proper framework to obtain an effective field theory that enables us to compute the physical observables by using *Green* Functions written in terms of the fields within the functional integral formalism [4, 5, 7, 8]. It allows the transformation of observables' complex quantum mechanical description into a more tractable one since we are translating the *Hamiltonian*'s dynamics at the microscopic level into a more manageable form that applies to a mesoscopic scale [4, 7].

Current Noise and Fluctuations

The phenomenon of quantum noise in electronic trans-

port arises from the intrinsic fluctuations in the flow of electrons, which are influenced by the quantum nature of charge carriers and their interactions [11].

Analyzing current-current correlations is an effective approach for comprehending and characterizing quantum noise since these correlations reflect the statistical interdependence of current at different points in time. Moreover, quantum phase transitions arise from quantum fluctuations, which become exceedingly significant and far-reaching at the quantum critical point. This phenomenon dominates the system's behavior, potentially destabilizing the mean-field states and rendering insufficient deterministic models and interaction-free approaches. These large fluctuations make the system span a wide range of states and induce non-linear effects that the saddle points cannot capture, significantly changing the system's properties.

In this work, we obtained the non-equilibrium zero-temperature phase diagram as a function of the interaction strength and applied voltage. Additionally, we have analyzed the behavior of charge susceptibility and current noise near the phase transition using the *Random Phase Approximation* (RPA). Finally, we have confirmed the validity of our results in the *Markovian* regime by employing the *Lindblad* equation.

II. MODEL AND METHODS

To explore charge noise near criticality, we employ a paradigmatic, tractable model featuring transport through an interacting quantum dot — which has the added advantage of being exactly solvable in the thermodynamic limit.

The system is comprised of an interacting quantum dot connected to metallic leads. The total Hamiltonian is given by

$$H = H_{\text{dot}} + H_{\text{dot-leads}} + H_{\text{leads}}, \quad (1)$$

here

$$H_{\text{dot}} = \sum_{\alpha=1}^M \varepsilon_{\alpha} d_{\alpha}^{\dagger} d_{\alpha} - \frac{\lambda}{M} \left(\sum_{\alpha=1}^M d_{\alpha}^{\dagger} d_{\alpha} - \frac{M}{2} \right)^2 \quad (2)$$

is the dot Hamiltonian with $\varepsilon_{\alpha=1,\dots,M}$ the individual energies of the dot's M levels and λ a negative charging energy around the half-filled condition. The coupling to the leads is given by

$$H_{\text{dot-leads}} = \frac{1}{\sqrt{V}} \sum_{l,\nu,k,\alpha} \left(c_{l\nu k}^{\dagger} \tau_{\nu,\alpha}^{(l)} d_{\alpha} + d_{\alpha}^{\dagger} \tau_{\alpha,\nu}^{(l)\dagger} c_{l\nu k} \right) \quad (3)$$

where $l = L, R$ labels the left or right lead, ν the transport channels of the leads and k the momentum of the electron. The Hamiltonian of the leads is given by $H_{\text{leads}} = \sum_{l,\nu,k} \Omega_{l,\nu,k} c_{l\nu k}^{\dagger} c_{l\nu k}$. As we consider metallic wide band leads, the details of the dispersion relation $\Omega_{l,\nu,k}$ are unimportant [10].

The lead l , taken to be infinite, is assumed to have been prepared in equilibrium, characterized by chemical potential μ_l and temperature T_l , before the coupling to the dot was turned on. In the following, we address the properties of the steady-state, where the transient regime has vanished.

When $\sum_{\alpha} \varepsilon_{\alpha} = 0$ the Hamiltonian of the isolated dot possesses particle-hole symmetry with respect to its chemical potential $\mu = 0$. However, for large enough λ the ground-state spontaneously breaks this symmetry. Since the number of particles on the dot commutes with the Hamiltonian, this transition is first order. In the presence of the leads, particle-hole symmetry is maintained for $\mu_L = \mu_R = V/2$ and symmetric coupling even in the presence of a finite bias (V). As shown in Fig. 1-(b), any finite dot-lead hybridization renders the symmetry breaking transition continuous.

It is convenient to take the energy levels of the dot to obey $\varepsilon_{\alpha} = \Lambda(-1 + (2\alpha - 1)/M)$, which ensues a constant density of states within the energy cutoff Λ . Nonetheless the results are qualitatively the same for other choices as long as particle-hole symmetry is preserved. We also take $\tau_{\nu,\alpha}^{(l)} = \tau \delta_{\nu,\alpha}$, i.e. each dot level tunnels to a transport channel with a different symmetry. Therefore, in the wide-band limit, the effects of the leads on the dot enter only through the hybridization matrix, $\Gamma_{\alpha,\alpha'} = \Gamma \delta_{\alpha,\alpha'}$, where $\Gamma \propto |\tau|^2 \rho(0)$, with $\rho(0)$ denoting the density of states of the leads.

In the following, we analyze the non-equilibrium phase diagram of the model, focusing on the charge fluctuations on the dot, the current and its fluctuations. This will be done using an action functional approach on the Keldysh contour.

A. Keldysh Action

To characterize the charge dynamics we consider the response $\chi^R(t, t') = -i \langle [N_d(t), N_d(t')] \rangle$ and fluctuation functions $\chi^K(t, t') = -i \langle \{N_d(t), N_d(t')\} \rangle$. $N_d = \sum_{\alpha} d_{\alpha}^{\dagger} d_{\alpha}$ is the total number of particles on the dot, and similarly, we define the number of particles in lead l as $N_l = \sum_{\nu,k} c_{l\nu k}^{\dagger} c_{l\nu k}$. We also study the current, which, with the convention $J_l = dN_l/dt = i[H, N_l]$, is explicitly given by

$$J_l = \frac{i}{\sqrt{V}} \sum_{\nu,k,\alpha} \left(c_{l\nu k}^{\dagger} \tau_{\nu,\alpha}^{(l)} d_{\alpha} - d_{\alpha}^{\dagger} \tau_{\alpha,\nu}^{(l)\dagger} c_{l\nu k} \right), \quad (4)$$

and its response $S_{l,l'}^R(t, t') = -i \langle [J_l(t), J_{l'}(t')] \rangle$ and fluctuation $S_{l,l'}^K(t, t') = -i \langle \{J_l(t), J_{l'}(t')\} \rangle$ dynamics. Specifically, we set $l = l' = L$ in what follows.

It is worth noting the differences between the current operator in Eq. (4) and the one typically considered in a *Landauer-Buttiker* approach. The current operator as defined above considers the measurement to occur near the lead in contrast with the Landauer-Buttiker formalism for which the current is measured inside the lead at a

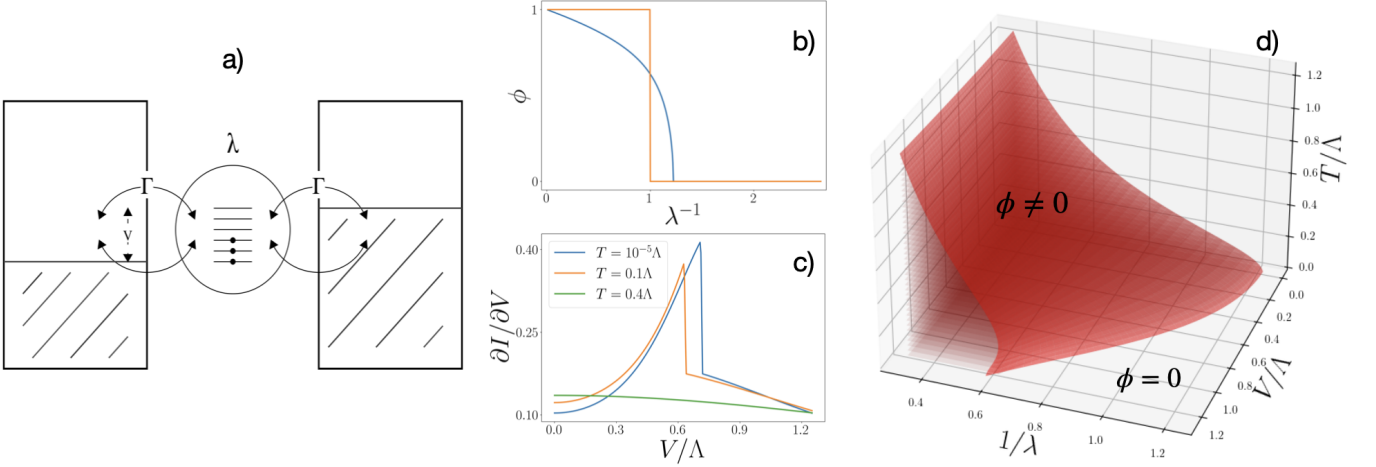


FIG. 1: Phase diagram; Current and Order parameters

large distance from the dot. Although the average value of the current should coincide in both cases, there are differences in current fluctuations.

We obtain the expressions for these observables, using a functional approach within the RPA approximation. To do this, we consider the generating function

$$Z[j, u] = \int Dc \int Dd e^{iS[j, u]} \quad (5)$$

where S , explicitly given by

$$\begin{aligned} S[j, u] = \int_C dz & \left[c^* g_c^{-1} c + d^* g_d^{-1} d + \frac{\lambda}{M} \left(N_d(z) - \frac{M}{2} \right)^2 \right. \\ & \left. - H_{\text{dot-leads}}(z) + j_l(z) J_l(z) + u(z) N_d(z) \right] \end{aligned} \quad (6)$$

is the action on the Keldysh contour where, g_c and g_d are the bare Green's functions of the leads and dot, respectively, and $j(z)$ and $u(z)$ are source fields conjugate to current and charge of the dot. (The convention of summing over repeated indices has been adopted.)

Decoupling the interacting term via the introduction of a bosonic Hubbard-Stratonovich decoupling field ϕ results in an effective action that is quadratic in the Grassmann fields. Integrating out the Grassmann fields results in a bosonic action given by

$$\begin{aligned} S[\phi, j, u] = -M \int_C dz \lambda & [\phi^2(z) + \phi(z)] \\ & - i \text{Tr} \ln \left[i \left(G_0^{-1} - \tilde{\Sigma}[j] + 2\lambda\phi - u \right) \right]. \end{aligned} \quad (7)$$

where

$$G_0^{-1} = g_d^{-1} - \Sigma_0, \quad (8)$$

$$\Sigma_0 = \frac{1}{V} \tau^\dagger g_0 \tau \quad (9)$$

$$\tilde{\Sigma}[j] = \frac{1}{V} \tau^\dagger (-ig_0 j + ijg_0 + jg_0 j) \tau. \quad (10)$$

In the following we perform a Keldysh rotation into classical and quantum variables where ϕ acquires a two component structure $\phi = (\phi^{cl}, \phi^q)^T$ and it is useful to define the matrix $\hat{\phi} = \phi^{cl} + \phi^q \sigma_1$ acting in Keldysh space, with σ_i ($i = 1, 2, 3$) are the Pauli Matrices.

B. Fluctuation Dissipation Ratios and Effective Temperature

The fluctuation-dissipation theorem links the response of a system in thermal equilibrium to its fluctuation spectrum which, in terms of Schwinger-Keldysh Green's functions, can be expressed as $Q_{\text{FDR}}(\omega) = \tanh(\beta\omega/2)$, which becomes a step function at $T = 0$ for correlators of bosonic fields. For nonthermal steady states, this generalizes to the fluctuation dissipation ratio (FDR) $Q_{\text{FDR}}^X = \Im \chi_X^R / \Im \chi_X^K$, with χ_X a correlator of observable X (e.g. charge: $X = N_d$), which, away from equilibrium, may not only depend on T and ω and the statistics of χ_X . The FDR of χ_X thus contains information about the linear-response regime, i.e., the regime where the system appears to be thermal. It also allows for a definition of an effective temperature T_{eff}^X in the nonlinear regime.

Interestingly, as we show in Appendix B, $Q_{\text{FDR}}^X(\Omega)$ can be measured by monitoring the occupation of an harmonic oscillator with frequency Ω weakly coupled to that observable, i.e. $H_{\text{HO}} = \Omega a^\dagger a + \eta X(a + a^\dagger)$. In the $\eta \rightarrow 0$ limit, we obtain (see Appendix B):

$$\langle a^\dagger a \rangle = \frac{1}{2} [Q_{\text{FDR}}^X(\Omega) - 1]. \quad (11)$$

The non-equilibrium FDR motivates the definition of an effective temperature

$$T_{\text{eff}}^X = \lim_{\omega \rightarrow 0} \frac{1}{2} [\partial_\omega Q_{\text{FDR}}^X(\omega)]^{-1}, \quad (12)$$

which can be seen as the temperature inferred from the

occupation of a harmonic oscillator with frequency $\omega \rightarrow 0$, weakly coupled to the X degrees of freedom of the dot.

C. Mean Field

The mean-field equations are obtained by minimizing the action of Eq. 7 with respect to ϕ , setting the sources u and j to zero. As the action globally scales with the number of levels on the dot, M , this saddle-point approximation becomes exact in the limit of large M ($M \rightarrow \infty$).

The self-consistent mean-field equations in the (time-translationally invariant) steady-state yield

$$\phi_0^{cl} = -\frac{i}{2M} \int \frac{d\omega}{2\pi} \text{tr} [\tilde{G}_0^K(\omega)], \quad (13)$$

and $\phi_0^q = 0$ where $\tilde{G}_0^K(\omega)$ is the Mean-Field Keldysh Green's function in the frequency domain and trace is performed over the dot's energy levels.

It is useful to introduce the mean-field single particle non-hermitian operator, $\mathbf{K} = H_{MF} - i\Gamma$, where $H_{MF} = \sum_\alpha d_\alpha^\dagger (\varepsilon_\alpha - 2\lambda\phi_0^{cl}) d_\alpha$ and Γ represents the coupling value to the leads. We assume the coupling of the left and right leads are the same, so $\Gamma = (\Gamma_L + \Gamma_R)/2 \equiv \Gamma$. With this notation, the mean-field Green's functions are given by

$$\tilde{G}_0^R(\omega) = [\tilde{G}_0^A(\omega)]^\dagger = (\omega - \mathbf{K})^{-1} = \sum_\alpha |\alpha\rangle \frac{1}{\omega - \lambda_\alpha} \langle \tilde{\alpha}|, \quad (14)$$

$$\tilde{G}_0^K(\omega) = -i\Gamma \sum_{l\alpha} |\alpha\rangle \frac{F_l(\omega)}{(\omega - \lambda_\alpha)(\omega - \lambda_\alpha^*)} \langle \alpha|, \quad (15)$$

where the labels R , A and K refer respectively to the *retarded*, *advanced* and *Keldysh Green's Functions*. The $|\alpha\rangle$ and $\langle \tilde{\alpha}|$ are the right and left eigenvectors of the \mathbf{K} operator, with eigenvalue λ_α . Here, \mathbf{K} basis is diagonal with $\lambda_\alpha = \varepsilon_\alpha - 2\lambda\phi_0^{cl} - i\Gamma$. $F_l(\omega) = \tanh \beta/2(\omega - \mu_l)$ encodes temperature and chemical potential of lead l . In what follows, the leads are held at the same temperature, i.e. $T_R = T_L = T$.

The non-equilibrium phase diagram as a function of the interaction strength, λ , temperature T , and bias voltage V is depicted in Fig. 1-(d). As already mentioned, we take the energy distribution of a dot to be constant, ranging from $-\Lambda/2$ to $\Lambda/2$, where $\Lambda = 2$ but confirmed that a different density of states respecting particle-hole symmetry gives the same qualitative results. The ordered phase that exists in equilibrium for a sufficiently large coupling constant can be destroyed in a continuous fashion either by increasing the temperature or the bias voltage. The conductance $G = dI/dV$ for different temperatures is given in Fig. 1-(c). Within the ordered phase upon increasing voltage G increases and passes by a discontinuity at the transition, decreasing with voltage in the disordered phase.

III. CHARGE SUSCEPTIBILITY

To obtain the charge susceptibility within RPA, we consider the fluctuation of the order parameter, $\delta\vec{\phi}^T = \vec{\phi}^T - \vec{\phi}_0^T$, around the saddle point value, $\vec{\phi}_0$ and neglect the current source, i.e. $j = 0$. In this approximation the action becomes

$$S_{\text{RPA}}[\phi, u] = \int dt \delta\vec{\phi}^T (2\lambda\chi_0) \vec{u} + \vec{u}^T (2\lambda\chi_0) \delta\vec{\phi} - \delta\vec{\phi}^T D^{-1} \delta\vec{\phi} - \vec{u}^T \chi_0 \vec{u}, \quad (16)$$

where

$$D^{-1} = \lambda(\sigma_1 + 4\lambda\chi_0), \quad (17)$$

is the inverse of the ϕ propagator, and the bare "bubble" is given by

$$\chi_0^{\alpha\beta}(t, t') = -\frac{i}{2} \text{Tr} [\tilde{G}_0(t, t') \gamma^\alpha \tilde{G}_0(t', t) \gamma^\beta]. \quad (18)$$

where α and β run over the *classical* (cl) and *quantum* (q) components and $\gamma^{cl} = I$ and $\gamma^q = \sigma_1$ are 2×2 matrices in the *Keldysh* space.

Integrating out the bosons and varying with respect to the sources, we get

$$\chi_{\text{RPA}}(z, z') = i\partial_{u(z)} \partial_{u(z')} \ln Z_{\text{RPA}} \quad (19)$$

with $\chi_{\text{RPA}} = \chi_0 (1 + 4\lambda\chi_0)^{-1}$, or in Keldysh space

$$\begin{aligned} \chi_{\text{RPA}} &= \begin{pmatrix} 0 & \chi_{\text{RPA}}^A \\ \chi_{\text{RPA}}^R & \chi_{\text{RPA}}^K \end{pmatrix} = \\ &= \begin{pmatrix} 0 & \chi_0^A (1 + 4\lambda\chi_0^A)^{-1} \\ \chi_0^R (1 + 4\lambda\chi_0^R)^{-1} & (1 + 4\lambda\chi_0^R)^{-1} \chi_0^K (1 + 4\lambda\chi_0^K)^{-1} \end{pmatrix}. \end{aligned} \quad (20)$$

The results for the charge susceptibility are shown in Fig. 2. Panels (a)-(c) show respectively the real and imaginary parts of the retarded susceptibility and the Keldysh component for several values of the voltage, at $V < V_c$, $V = V_c$ and $V > V_c$, both for $T = 0$ and $V = V_c$ at $T = 0.25\Lambda$. For each temperature, the values of λ , i.e., $\lambda/\Lambda = .5$ and $\lambda/\Lambda = .6$, were chosen to give the same critical voltage $V_c = .7\Lambda$ (see inset of (a) and color code therein). Both, response χ_{RPA}^R and correlation function χ_{RPA}^K , remain finite away from criticality but diverge for $\omega \rightarrow 0$, as $|\omega|^{-2}$, at the phase transition. As shown in Fig. 2-(d), as function of voltage, $\chi_{\text{RPA}}^R(\omega = 0)$ and $\chi_{\text{RPA}}^K(\omega = 0)$ diverge as $|V - V_c|^{-2}$ near the transition.

Fig. 2-(e) depicts the fluctuation dissipation ratios $Q_{\text{FDR}}^{N_d} = \Im \chi_{\text{RPA}}^R / \Im \chi_{\text{RPA}}^K$ as a function of frequency for the cases of panels (a)-(c). For any non-vanishing voltage, the derivative of $Q_{\text{FDR}}^{N_d}$ at $\omega = 0$ is finite. $Q_{\text{FDR}}^{N_d}$ interpolates between a strongly renormalized non-equilibrium value at small frequencies to its equilibrium form at the temperature of the leads for large frequencies. At zero

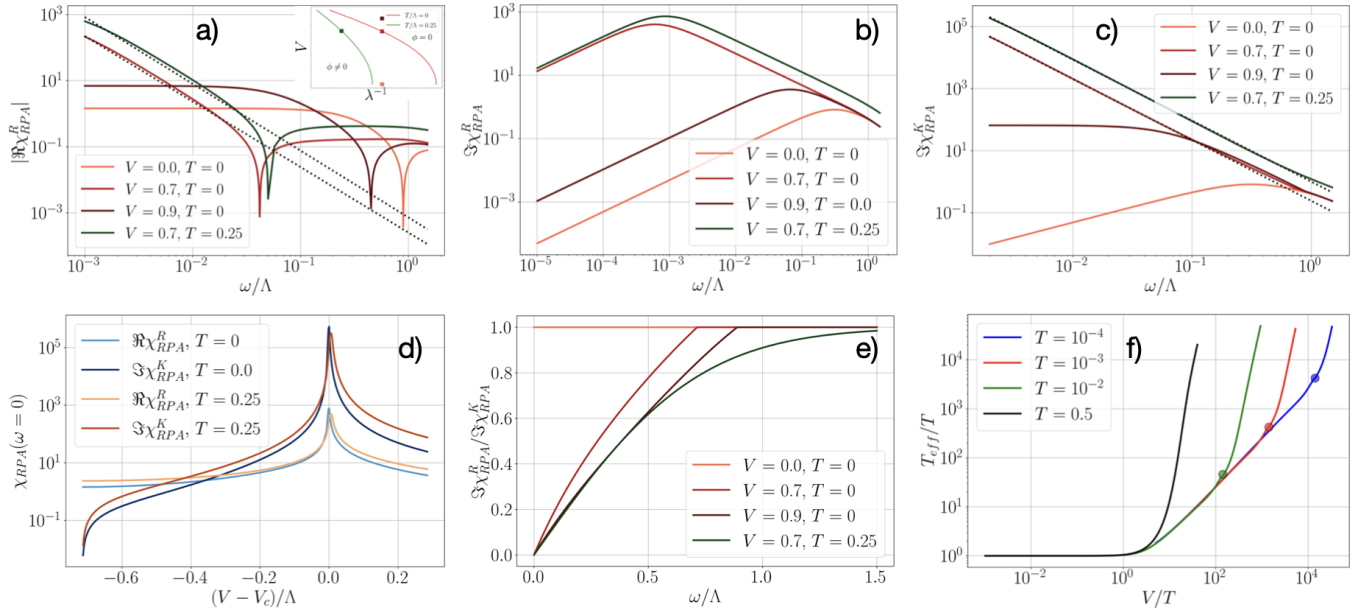


FIG. 2: Charge Susceptibility across the non-equilibrium phase transition: Real (a), imaginary (b) and Keldysh (c) components of the retarded RPA charge susceptibility for $T = 0$ and for $V = 0, V = V_c(T = 0)$ and $V > V_c(T = 0)$ (blue scale) and for $T > 0$ at $V_c(T)$. (d) - Values of the retarded and Keldysh components for $\omega = 0$ across the transition. (e) - Fluctuation dissipation ratios computed for the same values and color coding as (a-c). (f) - Effective Temperature determined from the FDR at zero frequency... [PR1: Inset labels of (a) too small; colors of the inset have to be the same as the lines of the main plot. legend of (d) standard and boring.]

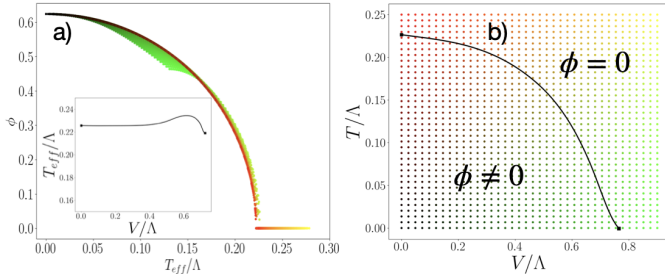


FIG. 3: Order parameter as a function of the effective temperature (a). Points are color-coded as in the phase diagram in panel (b). The inset shows the effective temperature along the critical line.

temperature, this passage arises at a non-analytical point for $\omega = V$. For finite temperature, this becomes a crossover scale at $\omega \sim V$.

Finally, Fig. 2-(f) depicts the effective temperature (Eq. 12) over the temperature of the leads as a function of V/T for several values of T . T_{eff} interpolates between T in equilibrium and a $\sim V^4$ behavior at large voltages. T_{eff} is non-analytic at $V = V_c(T)$ which can e.g. be inferred from panel (d). There are three qualitative regimes, a linear response regime $V < T$, where $T_{\text{eff}} \simeq T$; a non-linear response region $V > T, T_{\text{eff}} < T_C$; and the large bias limit $V \gg T, T > T_C$.

Interestingly, for the charge susceptibility we can show

(see Appendix C) that the FDR computed within RPA is the same as the bare one, i.e.

$$\frac{\Im\chi_{\text{RPA}}^R}{\Im\chi_{\text{RPA}}^K} = \frac{\Im\chi_0^R}{\Im\chi_0^K}. \quad (21)$$

This explains that $Q_{\text{FDR}}^{N_d}$ becomes non-analytic at the transition through dependence of χ_0 of the order parameter. This argument also shows that, at the RPA level, the effective temperature of the order parameter does not diverge at a non-equilibrium critical point even if its susceptibility diverges.

Fig. 3-(a) displays the order parameter ϕ as a function of the effective temperature T_{eff} for several representative points in the $V-T$ phase diagram (see color code in (b)). Strikingly, the data collapse onto a single curve near the transition, indicating that the behavior of ϕ in this regime may admit an equilibrium-like description when expressed in terms of T_{eff} rather than the actual temperature T .

IV. CURRENT NOISE

We now turn to the behavior of the current and its fluctuations across the non-equilibrium critical point. For this, we include the current source term j in the action and compute the average current and current noise via differentiation of the RPA action. Integration over the

bosonic *Gaussian Action*, in the presence of the current sources, we obtain

$$\ln Z_{\text{RPA}}[j] = iS_0[j] + \vec{A}_{[j]}^T iD \vec{A}_{[j]} - \frac{1}{2} \text{Tr} \ln iD^{-1}, \quad (22)$$

where $S_0[j]$ is the mean-field contribution, given by

$$S_0[j] = \int dt i\text{Tr} [\tilde{G}_0 \tilde{\Sigma}_0[j]] + \frac{i}{2} \text{Tr} [\tilde{G}_0 \tilde{\Sigma}_0[j] \tilde{G}_0 \tilde{\Sigma}_0[j]], \quad (23)$$

The interaction contributions are given in terms of the Keldysh vector

$$A^\alpha(t)_{[j]} = 2i\lambda \int dt_1 dt_2 \text{Tr} [\tilde{G}_0(t_1, t) \gamma^\alpha \tilde{G}_0(t, t_2) \tilde{\Sigma}_0[j](t_2, t_1)] \quad (24)$$

contracted with the bosonic propagator D .

A. Non-Interacting Contribution

We first consider the non-interacting contribution of the current noise, obtained by varying the mean-field contribution of Eq. (23):

$$\mathcal{S}_{0|L,L}^K(t, t') = \frac{1}{2} \frac{\delta^2 S_0[j]}{\delta j_L^q(t) \delta j_L^q(t')} \Big|_{j=0}, \quad (25)$$

where $j_L^c(t)$ ($j_L^q(t)$) is the *classical* (*quantum*) current source for the left lead at time t . Similarly, the corresponding response functions are given by:

$$\mathcal{S}_{0|L,L}^R(t, t') = \frac{1}{2} \frac{\delta^2 S_0[j]}{\delta j_L^q(t) \delta j_L^c(t')} \Big|_{j=0}. \quad (26)$$

$$\mathcal{S}_{0|L,L}^A(t, t') = \frac{1}{2} \frac{\delta^2 S_0[j]}{\delta j_L^c(t) \delta j_L^q(t')} \Big|_{j=0}. \quad (27)$$

The explicit expressions after performing the functional derivatives are given in the Appendix D. In the steady-state regime where time-translational invariance holds, we perform a Fourier transform to the frequency domain

$$\begin{aligned} \mathcal{S}_0^K(\omega) &= i \int \frac{d\nu}{2\pi} \text{Tr} [\tilde{G}_0(\nu^-) \sigma_1 \Sigma_0(\nu^+) \sigma_1] + \frac{i}{2} \int \frac{d\nu}{2\pi} \text{Tr} [\Sigma_0(\nu^+) \tilde{G}_0(\nu^+) \Sigma_0(\nu^+) \sigma_1 \tilde{G}_0(\nu^-) \sigma_1] \\ &+ \frac{i}{2} \int \frac{d\nu}{2\pi} [\tilde{G}_0(\nu^+) \sigma_1 \Sigma_0(\nu^-) \tilde{G}_0(\nu^-) \Sigma_0(\nu^-) \sigma_1] - \frac{i}{2} \int \frac{d\nu}{2\pi} \text{Tr} [\Sigma_0(\nu^+) \tilde{G}_0(\nu^+) \sigma_1 \Sigma_0(\nu^-) \tilde{G}_0(\nu^-) \sigma_1] \\ &- \frac{i}{2} \int \frac{d\nu}{2\pi} \text{Tr} [\tilde{G}_0(\nu^+) \Sigma_0(\nu^+) \sigma_1 \tilde{G}_0(\nu^-) \Sigma_0(\nu^-) \sigma_1], \end{aligned} \quad (28)$$

$$\begin{aligned} \mathcal{S}_0^A(\omega) &= i \int \frac{d\nu}{2\pi} \text{Tr} [\tilde{G}_0(\nu^-) \Sigma_0(\nu^+) \sigma_1] + \frac{i}{2} \int \frac{d\nu}{2\pi} \text{Tr} [\Sigma_0(\nu^+) \tilde{G}_0(\nu^+) \Sigma_0(\nu^+) \tilde{G}_0(\nu^-) \sigma_1] \\ &+ \frac{i}{2} \int \frac{d\nu}{2\pi} [\tilde{G}_0(\nu^+) \Sigma_0(\nu^-) \tilde{G}_0(\nu^-) \Sigma_0(\nu^-) \sigma_1] - \frac{i}{2} \int \frac{d\nu}{2\pi} \text{Tr} [\Sigma_0(\nu^+) \tilde{G}_0(\nu^+) \Sigma_0(\nu^-) \tilde{G}_0(\nu^-) \sigma_1] \\ &- \frac{i}{2} \int \frac{d\nu}{2\pi} \text{Tr} [\tilde{G}_0(\nu^+) \Sigma_0(\nu^+) \tilde{G}_0(\nu^-) \Sigma_0(\nu^-) \sigma_1], \end{aligned} \quad (29)$$

$$\mathcal{S}_0^R(\omega) = [\mathcal{S}_0^A(\omega)]^* \quad (30)$$

where the frequency arguments are given by: $\nu^\pm = \nu \pm \omega/2$.

An expression reminiscent of Eq. (28) has been reported by Liu et al. in the context of a topological superconductor coupled to normal metal leads [12].

B. Interacting Contribution

We now consider the interacting contribution to the current noise of the RPA action in Eq.(22). Varying the interaction term in order to the sources j , we obtain:

$$\mathcal{S}_{int|L,L}^K(t, t') = \frac{1}{2} \frac{\delta^2 \vec{A}_{[j]}^T D \vec{A}_{[j]}}{\delta j_L^q(t) \delta j_L^q(t')} \Big|_{j=0}, \quad (31)$$

and

$$\mathcal{S}_{int|L,L}^A(t,t') = \frac{1}{2} \frac{\delta^2 \vec{A}_{[j]}^T D \vec{A}_{[j]}}{\delta j_L^c(t) \delta j_L^q(t')} \Big|_{j=0}. \quad (32)$$

Explicitly in the steady-state, we get:

$$\begin{aligned} \mathcal{S}_{int}^K(\omega) &= -2\lambda^2 [D^K(\omega) T_+^{cl}(\omega) T_-^{cl}(\omega) + \\ &\quad D^R(\omega) T_+^{cl}(\omega) T_-^q(\omega) + D^A(\omega) T_+^q(\omega) T_-^{cl}(\omega)], \end{aligned} \quad (33)$$

$$\mathcal{S}_{int}^A(\omega) = -2\lambda^2 D^A(\omega) T_+^{cl}(\omega) K_-^q(\omega), \quad (34)$$

where we defined

$$T_\pm^\alpha = \mathcal{T}_1^{\alpha\pm} - \mathcal{T}_2^{\alpha\pm}, \quad (35)$$

$$K_\pm^\alpha = \mathcal{K}_1^{\alpha\pm} - \mathcal{K}_2^{\alpha\pm}, \quad (36)$$

with

$$\mathcal{T}_1^{\alpha\pm}(\omega) = \int \frac{d\nu}{\sqrt{2\pi}} \text{Tr} \left([\tilde{G}_0 \gamma^\alpha] (\nu^\pm) [\tilde{G}_0 \Sigma_0 \sigma_1] (\nu^\mp) \right), \quad (37)$$

$$\mathcal{T}_2^{\alpha\pm}(\omega) = \int \frac{d\nu}{\sqrt{2\pi}} \text{Tr} \left([\Sigma_0 \tilde{G}_0 \gamma^\alpha] (\nu^\pm) [\tilde{G}_0 \sigma_1] (\nu^\mp) \right), \quad (38)$$

$$\mathcal{K}_1^{\alpha\pm}(\omega) = \int \frac{d\nu}{\sqrt{2\pi}} \text{Tr} \left([\tilde{G}_0 \gamma^\alpha] (\nu^\pm) [\tilde{G}_0 \Sigma_0] (\nu^\mp) \right), \quad (39)$$

$$\mathcal{K}_2^{\alpha\pm}(\omega) = \int \frac{d\nu}{\sqrt{2\pi}} \text{Tr} \left([\Sigma_0 \tilde{G}_0 \gamma^\alpha] (\nu^\pm) [\tilde{G}_0] (\nu^\mp) \right), \quad (40)$$

where $\nu^\pm = \nu \pm \omega/2$. Although these analytic expressions are quite involved, the numerical evaluation of the expressions above is straightforward requiring only two one-dimensional integrals in frequency space. In the following, we study these integrals numerically to obtain the current noise in different regimes.

C. Results

We now discuss the current fluctuations obtained above. We start with the non-interacting limit ($\lambda = 0$). Current noise in this limit was first considered by Büttiker [11] for the case where the current is measured on the leads, asymptotically far away from the dot.

Figure 5 shows the correlation and response functions as a function of frequency. At low temperatures and small voltages, the zero-frequency current noise, $\Im S_0(\omega = 0)$, varies linearly with both V and T (see insets of panels (a) and (d)). While this behavior resembles the results obtained by Büttiker, the proportionality coefficients for shot noise, $\Im S_0(\omega = 0, T = 0) = s_V V$, and Nyquist noise, $\Im S_0(\omega = 0, V = 0) = s_T T$, differ from Büttiker's expressions due to the fact that current fluctuations are

measured near the quantum dot in our setup. Nonetheless, the results are qualitatively similar. In particular, for $T = 0$, $\Im S_0(\omega = 0)$ exhibits a non-analyticity at $\omega = V$, below which the effective temperature (as defined by the current fluctuation-dissipation relation) is finite, and above which $T_{\text{eff}}(\omega) = 0$ is recovered. At finite temperature, this non-analyticity is smoothed into a crossover around $\omega \sim V$, with $T_{\text{eff}}(\omega \ll V) \gg T$ and $T_{\text{eff}}(\omega \gg V) \simeq T$. In the absence of interactions, we also have that the effective temperatures obtained from the charge and current noise are qualitatively similar, differing at most by a factor of two for large voltages and low temperatures (see Fig. 4).

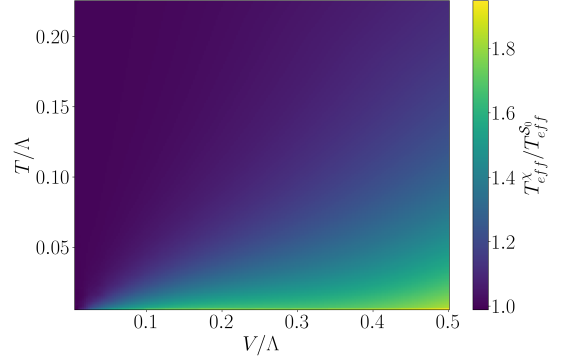


FIG. 4: Non-Interacting Current Noise and Charge Susceptibility effective temperature ratios

Now we turn to the interacting case. Fig. 6 shows the correlation and response functions as a function of frequency at the RPA level. In the disordered phase, the results resemble those for the non-interacting case discussed previously.

A striking difference with the non-interacting case is that within the ordered region, the imaginary part of the advanced component of the current noise correlator can become negative near zero frequency, while the imaginary part of the Keldysh component remains positive. This results in a negative effective temperature. Interpreting this result from an equilibrium perspective requires a population inversion.

Fig. 7 shows the effective temperature for $\omega = 0$ as a function of V and T . In the disordered phase T_{eff}^J is positive and diverges at the transition. This is to be contrasted with $T_{\text{eff}}^{N_d}$, which, although non-analytic, remains finite across the phase transition line. Within the ordered phase, T_{eff}^J is negative for sufficiently large V . For $V = 0$, $T_{\text{eff}}^J = T$ as required by the equilibrium fluctuation dissipation theorem. Interestingly, as V increases, T_{eff}^J decreases and becomes negative by crossing the $T_{\text{eff}}^J = 0$ line.

Again, a naive interpretation of these results from an equilibrium perspective would indicate that the system passes from populating uniquely its ground state to populating only the most excited states.

Far from the equilibrium transition at $T = T_c(V =$

0), there is a characteristic voltage, V_{flip} , for which the vanishing of T_{eff}^J takes place.

V. CONCLUSION

We investigate non-equilibrium phase transitions in a minimal quantum transport setup consisting of a particle-hole symmetric interacting quantum dot with a charging-energy term, tunnel-coupled to noninteracting leads. The fully connected character of the interaction renders the transition mean-field-like, even under finite bias voltage. We map out the non-equilibrium phase diagram as a function of temperature and voltage, and analyze its salient features. Our main results concern the behavior of the charge susceptibility and the current noise across the phase diagram.

We have established that the zero-frequency charge susceptibility diverges along the phase transition line as $|V - V_c|^{-\gamma}$ or $|T - T_c|^{-\gamma}$, with $\gamma = 2$, when crossing the transition along the voltage or temperature axes respectively.

We have computed the effective temperature that can be measured by the occupation of an Harmonic oscillator coupled to charge

We further confirmed the results of the average current and current noise using the *Lindblad* formalism in the high-voltage regime, where the system behaves in a *Markovian* manner. In this limit, both observables behave similarly to those in a non-interacting system, matching the interacting system's behavior at the RPA level in the same limiting regime.

These findings are significant because they demonstrate the value of current noise as a tool for detecting and probing critical fluctuations at quantum critical points, paving the way for studying other non-equilibrium voltage-driven transitions.

Appendix A: Markovian Regime

In the large voltage regime, the dot dynamics becomes Markovian [13], and the self-energy Σ_0 becomes delta-correlated. As a result, the dynamics is governed by a Lindblad equation, $\partial_t = \mathcal{L}[\rho]$, where ρ is the density matrix and the Lindbladian operator, \mathcal{L} , is given by:

$$\begin{aligned} \mathcal{L}[\rho] = & -i[H_{\text{dot}}, \rho] + \Gamma \sum_{\alpha} \left(d_{\alpha}^{\dagger} \rho d_{\alpha} - \frac{1}{2} \{ d_{\alpha}^{\dagger} d_{\alpha}, \rho \} \right) + \\ & + \Gamma \sum_{\alpha} \left(d_{\alpha} \rho d_{\alpha}^{\dagger} - \frac{1}{2} \{ d_{\alpha} d_{\alpha}^{\dagger}, \rho \} \right). \end{aligned} \quad (\text{A1})$$

This treatment is asymptotically exact for $V \rightarrow \infty$, where the jump operators, $\hat{L}_{R\alpha} = d_{\alpha}^{\dagger}$ and $\hat{L}_{L\alpha} = d_{\alpha}$, correspond to the hoping from the fully filled lead to the dot and from the dot to the completely empty lead.

The Markovian limit significantly simplifies the analysis of the current and its fluctuations [14], however the limit $V \rightarrow \infty$ restricts the analysis to the disordered regime. This helps explain why the current and current noise in the Markovian regime are the same as those obtained in the non-interacting case:

$$\langle \hat{J}_L \rangle = \frac{\Gamma}{2}, \quad (\text{A2})$$

$$\mathcal{S}(\omega) = \Gamma - \frac{2\Gamma^3}{4\Gamma^2 + \omega^2}. \quad (\text{A3})$$

These results agree with the those of Sec.IV A in the large V limit.

Appendix B: Harmonic Oscillator Thermometry

Let us consider a single bosonic mode at frequency Ω coupled to a large system. This could, i.e., be a local phonon coupled to the charge fluctuations on the dot of the main part. The generating function is given by

$$Z' = \int DX Da e^{iS[X] + i\{a^{\dagger} g_0^{-1} a - \eta \int_C dz X(z)[a(z) + a^{\dagger}(z)]\}}. \quad (\text{B1})$$

Considering a small η , at the lowest order we can write

$$\begin{aligned} Z' = & \int DX Da e^{iS[X] + i\{a^{\dagger} g_0^{-1} a - \eta \int_C dz X(z)[a(z) + a^{\dagger}(z)]\}} \\ \simeq & \int Da e^{i\{a^{\dagger} g_0^{-1} a - \frac{\eta^2}{2}[a+a^{\dagger}]X[a+a^{\dagger}]\}} \end{aligned} \quad (\text{B2})$$

$$= \int Da e^{i \int \frac{1}{2} A^{\dagger}(z) G(z, z') A(z')} \quad (\text{B3})$$

where $\chi(z, z') = -i \langle X(z) X(z') \rangle$ is the contour-ordered correlator of the field the boson is coupled to. The last equality is obtained by writing the action in Nambu space $A = \{a, a^{\dagger}\}^T$, where the propagator given by

$$G(z, z') = \begin{pmatrix} g_0^{-1}(z, z') - \eta^2 \chi(z, z') & -\eta^2 \chi(z, z') \\ -\eta^2 \chi(z, z') & g_0^{-1}(z', z) - \eta^2 \chi(z, z') \end{pmatrix}.$$

In the long-time limit when the system will have *thermalized* to its non-equilibrium steady-state limit, where time-translational invariance applies. In this limit and at the order of interest in η , the anomalous terms of the propagator vanish. Therefore, it is sufficient to consider the diagonal part given by

$$g^R(\omega) = [\omega - \Omega - \eta^2 \chi^R(\omega)]^{-1}, \quad (\text{B4})$$

$$g^K(\omega) = \frac{-\eta^2 \chi^K(\omega)}{[\omega - \Omega - \eta^2 \chi^R(\omega)][\omega - \Omega + \eta^2 \chi^A(\omega)]}. \quad (\text{B5})$$

For the Keldysh component we now use the identity $\lim_{\gamma \rightarrow 0} \frac{\gamma/\pi}{x^2 + \gamma^2} = \delta(x)$ with $\gamma = \eta^2 \chi''(\omega)$. This yields

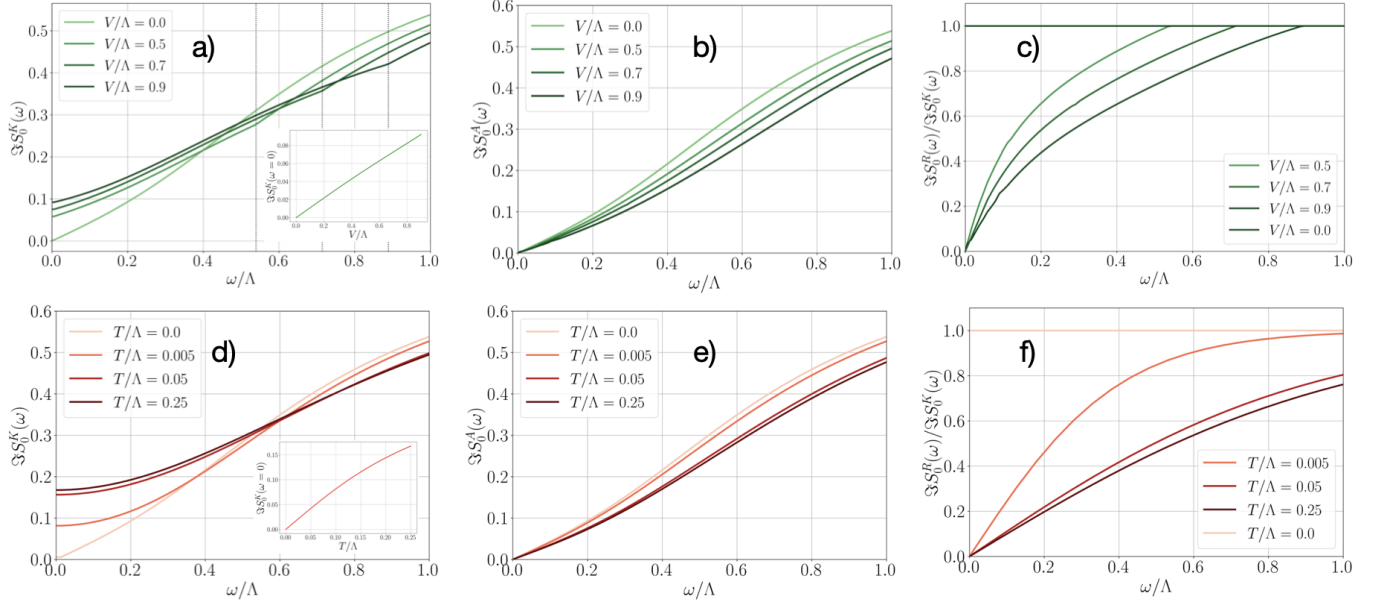


FIG. 5: Non-Interacting Current Noise

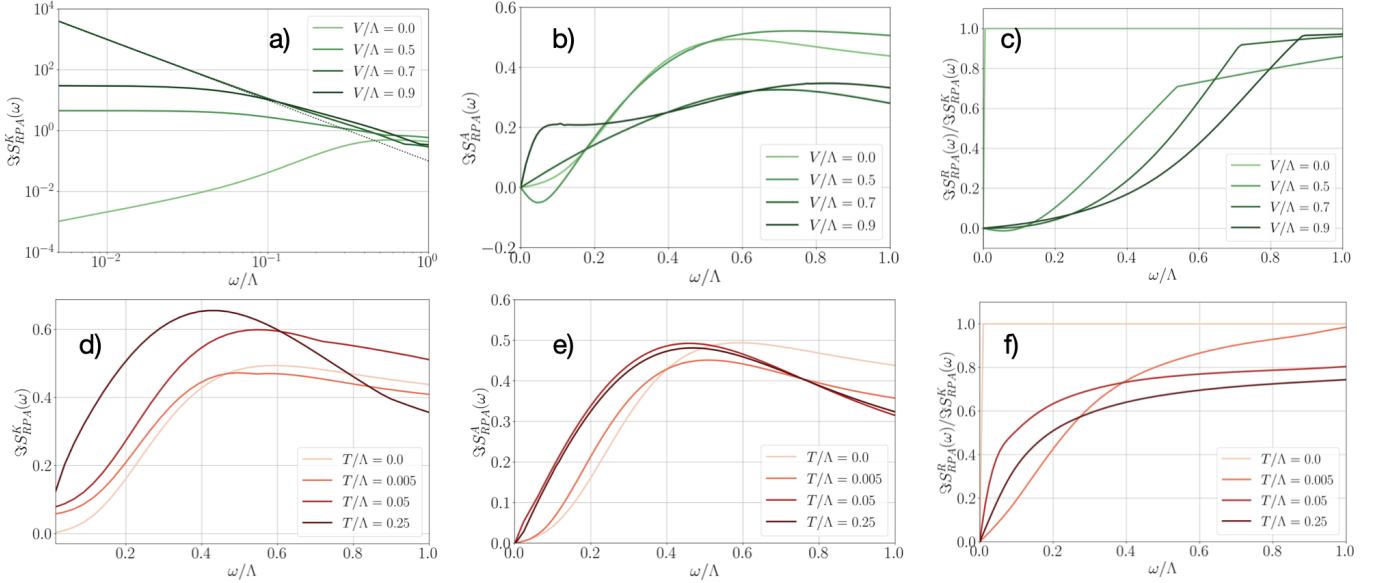


FIG. 6: RPA Current Noise

$g^K(\omega) = -2i\pi Q_{FDR}^\chi(\Omega) \delta(\omega - \Omega)$, where $Q_{FDR}^\chi = \chi^K / (\chi^R - \chi^A)$ is the fluctuation dissipation ratio of χ . The occupation of the bosonic level in the steady-state

$$\langle a^\dagger a \rangle = \frac{1}{2} \left[i \int \frac{d\omega}{2\pi} g^K(\omega) - 1 \right] = \frac{1}{2} [Q_{FDR}^\chi(\Omega) - 1].$$

It is worth noting that in equilibrium $Q_{FDR}^\chi(\Omega) = \tanh^{-1}\left(\frac{\beta\Omega}{2}\right)$, which simply states that the occupation is given in terms of the (equilibrium) Bose function at temperature $1/\beta$.

Appendix C: FDR for the RPA charge susceptibility

The fact that the RPA FDR and the bare one yield the same result can be simply obtained observing that

$$\frac{\Im \chi_{RPA}^K}{\Im \chi_{RPA}^R} = \frac{\Im \left[\frac{\chi_0^K}{(1+4\lambda\chi_0^R)(1+4\lambda\chi_0^A)} \right]}{\Im \left[\frac{\chi_0^R(1+4\lambda\chi_0^A)}{(1+4\lambda\chi_0^R)(1+4\lambda\chi_0^A)} \right]} = \frac{\Im \chi_0^K}{\Im \chi_0^R},$$

where we used $(\chi_0^R)^* = \chi_0^A$ and thus:

$$\Im [(1+4\lambda\chi_0^A)(1+4\lambda\chi_0^R)] = 0.$$

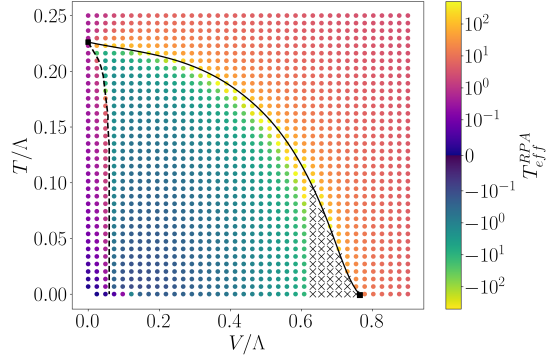


FIG. 7: Current Noise Diagrams

Appendix D: Explicit expressions of Current Noise correlations and response functions

After performing the functional derivatives in Eqs. (25, 27) and reorganizing the expression, we obtain for the non-interacting contribution in the time domain

$$\begin{aligned} \mathcal{S}_0^K(t, t') = & i\text{Tr}[(G_0\sigma_1)(t', t)(\Sigma_0\sigma_1)(t, t')] + \frac{i}{2}\text{Tr}[(\Sigma_0G_0\Sigma_0\sigma_1)(t', t)(G_0\sigma_1)(t, t')] + \frac{i}{2}\text{Tr}[(G_0\sigma_1)(t', t)(\Sigma_0G_0\Sigma_0\sigma_1)(t, t')] \\ & - \frac{i}{2}\text{Tr}[(\Sigma_0G_0\sigma_1)(t', t)(\Sigma_0G_0\sigma_1)(t, t')] - \frac{i}{2}\text{Tr}[(G_0\Sigma_0\sigma_1)(t', t)(G_0\Sigma_0\sigma_1)(t, t')], \end{aligned} \quad (\text{D1})$$

and

$$\begin{aligned} \mathcal{S}_0^A(t, t') = & i\text{Tr}[G_0(t, t')(\Sigma_0\sigma_1)(t', t)] + \frac{i}{2}\text{Tr}[(\Sigma_0G_0\Sigma_0)(t', t)(G_0\sigma_1)(t, t')] + \frac{i}{2}\text{Tr}[(G_0)(t, t')(\Sigma_0G_0\Sigma_0\sigma_1)(t', t)] \\ & - \frac{i}{2}\text{Tr}[(\Sigma_0G_0)(t', t)(\Sigma_0G_0\sigma_1)(t, t')] - \frac{i}{2}\text{Tr}[G_0\Sigma_0(t', t)(G_0\Sigma_0\sigma_1)(t, t')]. \end{aligned} \quad (\text{D2})$$

In the context of the expressions for interacting components of Current Noise, we begin with the following:

$$\vec{A}_{[j]}^T D \vec{A}_{[j]} = -4\lambda^2 \int dt_1 dt_2 A_{[j]}^\alpha(t_1) D_{\alpha\beta}(t_1, t_2) A_{[j]}^\alpha(t_2). \quad (\text{D3})$$

After calculating the $\delta A^\alpha(t_1)/\delta j_L^\beta(t_2)$ using Eq.(24), we consistently find a set of terms that exhibit the same temporal and causal structure, which is represented by:

$$\mathcal{S}_{\text{aux}}^{\alpha\beta}(t, t') = 2\lambda^2 \int dt_1 dt_2 D_{\alpha\beta}(t_1, t_2) \text{Tr}[M_1^\alpha(t, t_1) M_2(t_1, t)] \text{Tr}[N_1^\beta(t', t_2) N_2(t_2, t')], \quad (\text{D4})$$

where we should consider M_1^α and N_1^α as the first blocks of Green functions in Eqs. (37 - 40). They could correspond to either $[\tilde{G}_0\gamma^\alpha]$ or $[\Sigma_0\tilde{G}_0\gamma^\alpha]$, depending on the specifics of Σ_0 and the Keldysh nature of the current source j (whether it is classical or quantum). Following the same reasoning, M_2 and N_2 correspond to the second blocks in Eqs. (37 - 40) and may be represented by one of the following: $[\tilde{G}_0\Sigma_0\sigma_1]$, $[\tilde{G}_0\sigma_1]$, $[\tilde{G}_0\Sigma_0]$, or $[\tilde{G}_0]$.

In the steady-state and frequency domain, the expressions for $\mathcal{S}_{\text{aux}}^{\alpha\beta}$ always exhibit the same frequency structure, which is given by:

$$\mathcal{S}_{\text{aux}}^{\alpha\beta}(\omega) = 2\lambda^2 D_{\alpha\beta}(\omega) \int \frac{d\nu_1}{\sqrt{2\pi}} \text{Tr}[M_1^\alpha(\nu_1^+) M_2(\nu_1^-)] \int \frac{d\nu_2}{\sqrt{2\pi}} \text{Tr}[N_1^\beta(\nu_2^+) N_2(\nu_2^-)]. \quad (\text{D5})$$

By applying this to $\mathcal{S}_{\text{int}}^K$ and $\mathcal{S}_{\text{int}}^A$, and after performing some algebraic manipulations, we derive the expression presented in Eqs. (33, 34).

[1] S. Datta, *Quantum Transport: Atom to Transistor* (Cambridge University Press, 2005).

[2] D. Ventra, *Electrical Transport in Nanoscale Systems*

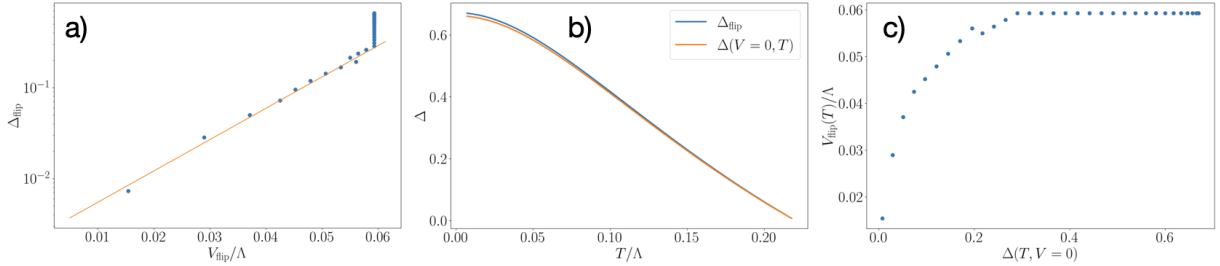


FIG. 8: Gap features

- (Cambridge University Press, 2002).
- [3] H.-P. Breuer and F. Petruccione, *The Theory of Open Quantum Systems* (Oxford University Press, 2002).
 - [4] M. F. Maghrebi and A. V. Gorshkov, Nonequilibrium many-body steady states via keldysh formalism, *Physical Review B*, 93(1), 014307 (2016).
 - [5] A. Kamenev, *Field Theory of Non-Equilibrium Systems* (Cambridge University Press., 2011).
 - [6] L. V. Keldysh, Diagram technique for nonequilibrium processes, *J. Exptl. Theoret. Phys. (U.S.S.R.)* 47, 1515-1527 (1965).
 - [7] L. M. Sieberer, M. Buchhold, , and S. Diehl, Keldysh field theory for driven open quantum systems, arXiv (2016).
 - [8] P. Ribeiro, Non-equilibrium current spectroscopy near a magnetic critical point () .
 - [9] P. Ribeiro, Green's function approach to many body systems out of equilibrium — applications to transport — () .
 - [10] P. Ribeiro, A. E. Antipov, and A. N. Rubtsov, Nonequilibrium breakdown of a correlated insulator through pattern formation, *PHYSICAL REVIEW B* 93, 144305 (2016).
 - [11] Y. M. Blanter and M. Büttiker, Shot noise in mesoscopic conductors, *Physics Reports*, 336(1-2), 1-166 (2000).
 - [12] L. et al., Probing majorana physics in quantum dot shot noise experiments, arXiv (2018).
 - [13] P. Ribeiro and V. R. Vieira, Non-Markovian effects in electronic and spin transport, *Physical Review B* **92**, 100302 (2015).
 - [14] L. et al., Current fluctuations in open quantum systems: Bridging the gap between quantum continuous measurements and full counting statistics, arXiv (2024).
 - [15] R. van Leeuwen et al., *Introduction to the Keldysh Formalism, Lect. Notes Phys.* (Springer-Verlag, 2006).
 - [16] J. Maciejko, *An Introduction to Nonequilibrium Many-Body Theory* (Springer, 2007).
 - [17] A. Kamenev, *Many-Body Theory of Non-Equilibrium*

- Systems* (2005).
- [18] A. Kamenev and A. Levchenko, Keldysh technique and nonlinear sigma model: Basic principles and applications, *Advances in Physics*, 58(3), 197-319 (2009).
 - [19] S. Sachdev, *Quantum Phase Transitions* (Cambridge University Press., 2011).
 - [20] D. Tong, Kinetic theory: University of cambridge graduate course (2012).
 - [21] M. Vojta, Quantum phase transitions, *Reports on Progress in Physics*, 66(12), 2069 (2003).
 - [22] P. Coleman and A. J. Schofield, Quantum criticality, *Nature*, 433(7023) (2005).
 - [23] G. R. Stewart, Non-fermi-liquid behavior in d- and f-electron metals, *Reviews of Modern Physics*, 73(4), 797 (2001).
 - [24] K. et al., Electron transport in quantum dots, *R* (1997).
 - [25] K. et al., Few-electron quantum dots, *Reports on Progress in Physics*, 64(6), 701-736 (2001).
 - [26] V. der Wiel and W. G. et al., Electron transport through double quantum dots, *Reviews of Modern Physics*, 75(1), 1 (2002).
 - [27] C. Emary, Theory of nanostructures, *Lecture Notes* (2009).
 - [28] Y. V. Nazarov and Y. M. Blanter, *Quantum Transport: Introduction to Nanoscience* (Cambridge University Press, 2009).
 - [29] C. P. Zelle, R. Daviet, A. Rosch, and S. Diehl, Universal phenomenology at critical exceptional points of nonequilibrium o(n) models, arXiv (2023).
 - [30] N. Kunwar, H. Zala, and K. Parveen, *Quantum Dots: Fundamentals, Synthesis, and Applications* (Elsevier, 2022).
 - [31] D. A. Paz and M. F. Maghrebi, Time-reversal symmetry breaking and emergence in driven-dissipative ising models, *SciPost Phys.* 12, 066 (2022).